

Cyclic voltammetric studies on zinc transition metal alloy electrodeposition

V. Ravindran* and V. S. Muralidharan

Cyclic voltammetric studies were carried out on zinc transition metal alloy films to identify the phases formed during alloy deposition. The deposition of zinc was found to involve stepwise reduction of divalent zinc ions. The formation of monovalent zinc ion was found to be slow. The zinc alloy systems were found to be anomalous, resulting in a higher content of zinc in the film. Dissolution of zinc from the alloy was observed. The dissolution was found to occur in intermediate phases rich in zinc.

Keywords: Cyclic voltammetry, Electrodeposition, Intermediate phases, Zinc alloys

Introduction

As early as 1928, an electrochemical technique based on the dissolution characteristics of plated samples was developed for the thickness of metallic coating.¹ Using this method of analysis, it was possible to determine the thickness of the coating and that of the intermediate layer between the coating and the base metal, which usually consists of various phases, as well as to obtain data about the phase structure.² This is the first attempt by an electrochemical technique. Different electrochemical techniques such as galvanostatic,^{3,4} potentiostatic⁵⁻⁷ and cyclic voltammetry^{8,9} have been used. Bolometric methods of analysis for phase identification are also discussed.¹⁰ Giriene *et al.* have studied the corrosion behaviour of Zn and Zn alloy coatings in alkaline media.¹¹ Studies of corrosion resistance under simulated conditions and field exposure of multilayered zinc-nickel and zinc-cobalt alloys have been made by M. Pushpavanam and M. Siluvai.¹² Ivaškevič *et al.* have investigated selective dissolution of electrodeposited Zn-Ni alloy coatings.¹³ Zinc-cobalt compositionally modulated alloy multilayer coatings were studied by A. M. E. Bahrololoom, D. R. Gabe and G. D. Wilcox.¹⁴

The present communication describes cyclic voltammetric experiments on zinc-cobalt, zinc-nickel and zinc-iron alloy systems, which show anomalous electrodeposition.

Experimental

Triangular potential sweep voltammetry was carried out using a proprietary potentiostat/galvanostat system (PAR EG&G, Princeton, NJ, USA). A conventional three electrode assembly, consisting of glassy carbon (0.2 cm²) as the working electrode, platinum as the counter electrode and a saturated calomel electrode as the reference electrode, was used. The working electrode was kept at extreme negative potentials for 1 min. The

solutions under study were deoxygenated for 1 h using purified hydrogen. The chemicals used were of Analar grade. The temperature of the cell was kept at 30°C. The pH values of the solutions were adjusted using a digital pH meter (Philips). Structural characterisation of the deposit was carried out by X-ray diffraction (XRD) using a JEOL JDX 803 diffractometer. The samples were scanned at 30–80° (2θ) at a scan rate of 1° min⁻¹ using Cu K_α (λ=1.5405 Å) radiation. The peaks due to different phases were identified and the corresponding lattice parameters were calculated.

Electrodeposition

Cold rolled mild steel plates (10 × 7.5 × 0.05 cm) were degreased with trichloroethylene and alkaline electro cleaned cathodically for 2 min in a solution of 35 g L⁻¹ NaOH and 25 g L⁻¹ Na₂CO₃ at 70°C. They were washed in running water and dipped in 5% H₂SO₄ solution for 10 s. Finally, they were washed with deionised water.

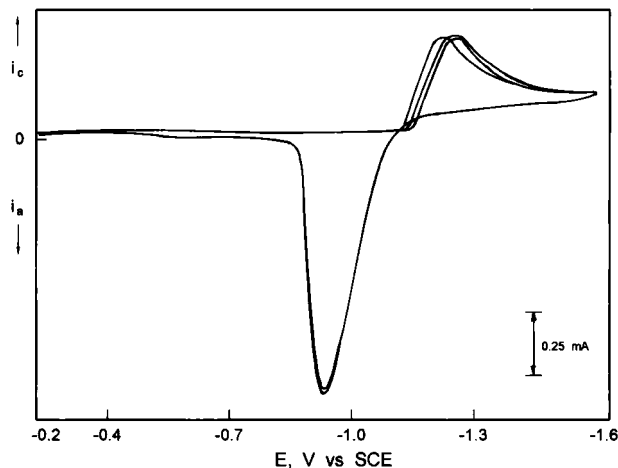
Electrodeposition was carried out using a pure zinc (99.99%) anode and a steel cathode in an 800 mL solution, in a 1 L wide mouthed vessel. The detailed composition and conditions of electrodeposition are shown in Table 1.

Results

Figure 1 presents the cyclic voltammograms obtained in 0.5M Na₂SO₄ solutions containing ZnSO₄ at 20 mV s⁻¹. An excursion of potential from -1600 to -200 mV revealed an anodic peak at -900 mV, while a distinct cathodic peak was seen at -1200 mV in the reverse scan. On repeated cycling, the anodic peak potential remained the same while the cathodic peak potentials became more negative, indicating that reduction becomes more difficult. The anodic peak potentials became more noble with the sweep rate ν and the cathodic peak potentials varied with ν , $(d \log E_{p,c} / d \log \nu)_\nu = 0.35$ was observed. A decade change of ZnSO₄ concentration caused the peak currents to vary and $\{d \log i_{p,c} / d \log [Zn^{++}]\}_{pH} = 0.9$.

Central Electrochemical Research Institute, Karaikudi 630 006, India

*Corresponding author, email visalakshi47@yahoo.com



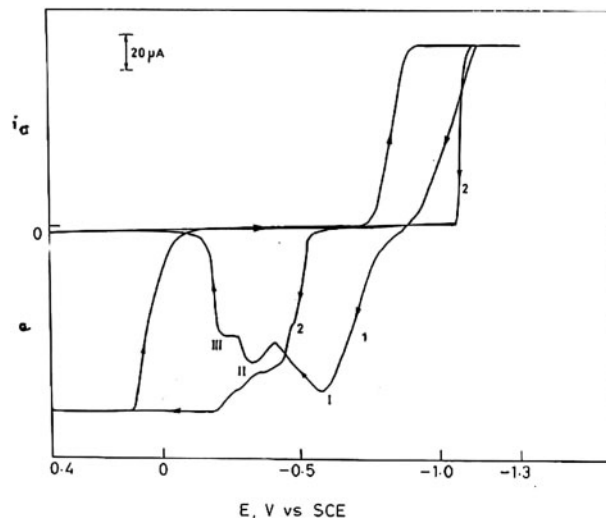
1 Cyclic voltammograms obtained in 0.5M ZnSO₄+0.5M Na₂SO₄ solutions, at $\nu=20 \text{ mV s}^{-1}$

Figure 2 shows the cyclic voltammograms obtained in 0.5M ZnSO₄+0.5M CoSO₄+0.5M Na₂SO₄ solutions, at 20 mV s⁻¹. An excursion of potential from -1300 to 400 mV revealed interesting features. During the forward scan, three well defined peaks appeared at -650 (I), -400 (II) and -140 mV (III). The reverse scan showed no cathodic peak. The second cycling caused the anodic peaks to merge after -400 mV. The anodic potentials varied as 125, 138 and 62 mV per decade change of sweep rates.

Figure 3 gives the cyclic voltammograms obtained in sulphamate solutions with different Zn/Ni molar ratios at 20 mV s⁻¹. When polarised from -2000 to 500 mV, the forward scan showed a small peak at -280 mV (0.1:0.9 solutions). The current started increasing beyond -1260 mV in the reverse scan. When the Zn/Ni concentration ratios varied, during the forward scan, a small shoulder appeared around -900 mV, which was followed by a peak at -240 mV. The reverse scan showed a plateau at -1450 mV. In solutions with Zn/Ni ratio of 0.5:0.5, the plateau around -760 mV widened, while splitting of the peak occurred at -80 mV. In

Table 1 Composition and conditions of electrodeposition

Bath	Composition and conditions
Zinc-nickel	0.5M zinc sulphamate 0.5M nickel sulphamate 50 g L ⁻¹ boric acid 0.345 g L ⁻¹ sodium lauryl sulphate 30 min, 50°C, with constant stirring
Zinc-cobalt	0.6M ZnSO ₄ 0.9M CoSO ₄ 45 g L ⁻¹ NH ₄ Cl 0.5M Na ₂ SO ₄ 40 g L ⁻¹ boric acid 0.865 g L ⁻¹ sodium lauryl sulphate 0.345 g L ⁻¹ β -naphthol 30 min, 55–60°C, with constant stirring
Zinc-iron	0.05M zinc sulphate 0.01M ferrous ammonium sulphate 20 g L ⁻¹ sodium sulphate 30 g L ⁻¹ boric acid 0.12M methanol 0.2M triethanolamine 0.0025M ascorbic acid 0.06M sodium lauryl sulphate 30 min, room temperature, with constant stirring



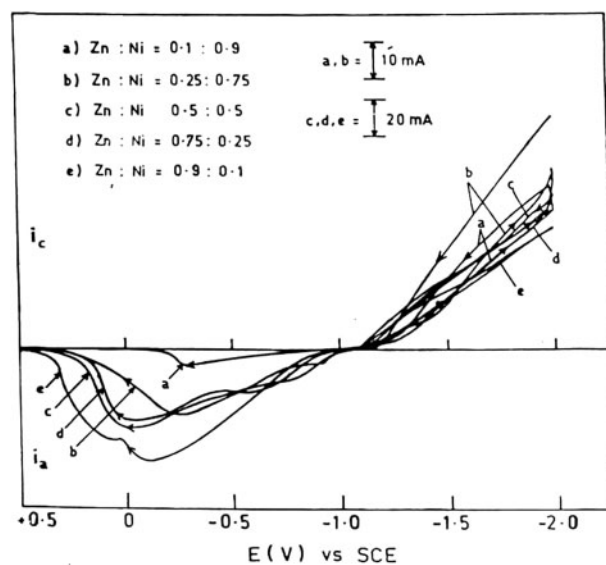
2 Cyclic voltammograms obtained in 0.5M ZnSO₄+0.5M CoSO₄+0.5M Na₂SO₄ solutions, at $\nu=20 \text{ mV s}^{-1}$

solutions with Zn/Ni ratio of 0.75:0.25, a rise of zinc concentration caused the peak potentials to shift to -120 mV.

Figure 4 presents the cyclic voltammograms obtained in the solutions of Zn/Fe molar concentration of 1:1, at various sweep rates. During the forward scan, the zero current crossing potential appeared at -1263 mV. The anodic peak potentials were invariant, while the cathodic peak potentials became active with sweep rate and varied as 40 mV per decade change of sweep rate.

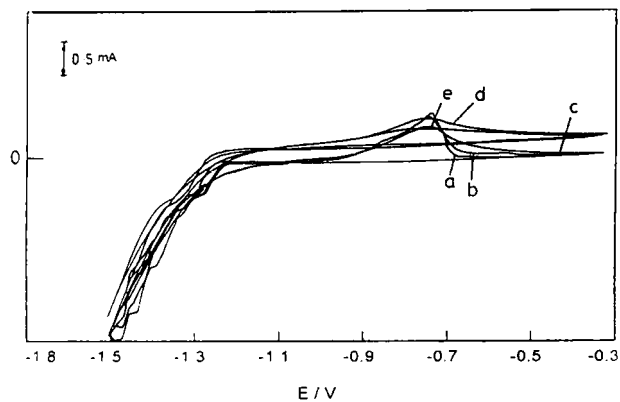
Discussion

Constant potential or potential sweep conditions are essential for a quantitative determination of the phase composition. It is important that the entire film dissolves so that the diffusion of the alloy constituents in the solid phase does not influence the process of diffusion. The use of solutions of simple and complex salts, such as



a Zn/Ni=0.1:0.9; b Zn/Ni=0.25:0.75; c Zn/Ni=0.5:0.5; d Zn/Ni=0.75:0.25; e Zn/Ni=0.9:0.1

3 Cyclic voltammograms obtained in sulphamate solutions with different Zn/Ni molar ratios, at $\nu=20 \text{ mV s}^{-1}$



a 5 mV s⁻¹; b 10 mV s⁻¹; c 20 mV s⁻¹; d 50 mV s⁻¹; e 100 mV s⁻¹

4 Cyclic voltammograms obtained in solutions of Zn/Fe molar concentration of 1:1, at various sweep rates

Na₂SO₄ and sodium citrate, helps in the depassivation of the alloy surface.

When a single phase binary alloy is anodically dissolved,¹⁵ the mechanism of dissolution may be:

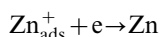
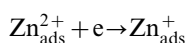
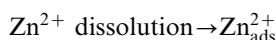
- (i) simultaneous dissolution of both components of the alloy, with the more noble one being reprecipitated on the spot
- (ii) partial dissolution of the less noble component, causing restructuring of the remaining matrix into a phase richer in the more noble component
- (iii) complete dissolution of the less noble component, with the atoms of the more noble component getting aggregated by surface diffusion: formation of patches and monolayers of the more noble component, with the possibility of formation of three-dimensional crystals, which may prevent further dissolution of the less noble component.

The mechanism of alloy dissolution depends on the composition. At low content of more noble metals, the dissolution of the less noble one leaves the atoms of the former loose and ready to dissolve (oxidise). Conversely, at high contents of the more noble metal, the atoms of the less noble one are likely to get squeezed out of the lattice, without producing many changes in the latter. Dissolution of one alloy phase from a mixture with other phases must suffer transport difficulties. The dissolution current comes under diffusion control, which makes the current-potential patterns similar to that obtained in such a situation for a cathodic metal deposition process. Hence it shows a maximum and subsequently, a decay.

Deposition and dissolution of zinc

In ZnSO₄ solutions, the deposition of zinc under transient polarization conditions (5–100 mV s⁻¹) may involve the formation of Zn⁺ and Zn⁺⁺ ions.

Deposition of zinc may take place as



If the first electron transfer step is slow

$$\vec{i}_c = \frac{\vec{k}_1}{\vec{k}_2} [\text{Zn}^{2+}] \exp\left(-\frac{\alpha_c F \Delta \phi c}{RT}\right)$$

where α_c is the cathodic transfer coefficient; $\Delta \phi$ is the interfacial potential difference, \vec{k}_1 and \vec{k}_2 are the forward and backward rate constants, and RT is room temperature.

If the discharge is irreversible^{16,17}

$$E_{p,c} = E_c^o + \frac{RT}{nF} \left[\frac{\ln k^o}{D^{1/2}} - 0.5 \ln \left(\frac{\alpha_c F v}{RT} \right) - 0.78 \right]$$

where $E_{p,c}$ is the cathodic peak potential, E_c^o is the equilibrium potential, k^o is the equilibrium rate constant, v is the sweep rate and D is the diffusion coefficient of Zn⁺⁺ ions. A plot of $E_{p,c}$ v. $\log v$ would give a straight line. An observed cathode Tafel slope of 140 mV/decade confirms this.

Deposition of zinc alloy

Brenner¹⁸ classified codeposition as anomalous where there is a preferential deposition of the less noble metal, the deposition of the less noble metal being suppressed by the preferential deposition of hydroxides of the less noble metal. An idea based on work function¹⁹ suggests that if the work function of the alloy lies between that of the parent metals, then continuous underpotential of the metal is possible.

Anomalous codeposition of zinc alloys may be due to:

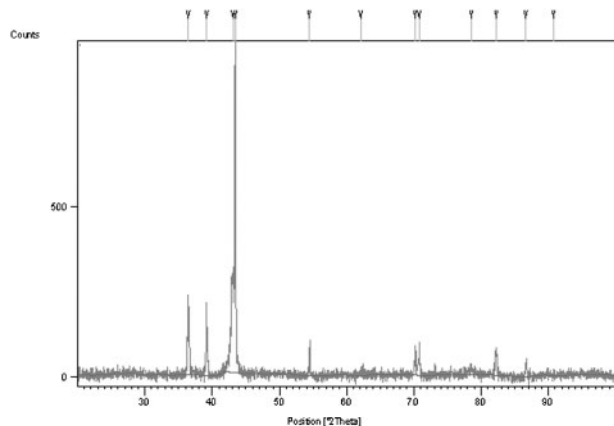
- (i) an increase in surface pH causing the formation of Zn(OH)₂ which may suppress the discharge of noble metals (Fe or Co or Ni)
- (ii) zinc deposition may be controlled by mass transport, and noble deposition by kinetic control
- (iii) the rate of charge transfer of ZnOH⁺ or MOH⁺ where M may be Fe or Co or Ni
- (iv) the monolayer coverage of noble metal may be followed by water molecules chemisorption with the creation of MOH_{ads}.

In the case of anomalous deposition of zinc alloys, many zinc atoms may get trapped on the spot of the growing phase creating distortions and other types of faults in the crystal lattice, which otherwise has no affinity to accommodate them. This phase becomes a supersaturated solid solution or an intermediate phase for the particular composition.

Dissolution of alloy film

Electrodeposited alloys obtained at low temperatures, unlike thermal or cast alloys, may not have phases predicted by phase diagrams. To do so, the phase diagram should be examined in the low temperature region. However, predictions cannot be made with certainty because electrodeposits are often fine grained and the fine crystal sizes may promote greater solubility than estimated by a phase diagram. Therefore, deviations from such diagrams may be expected. A structure obtained electrically may be different from those obtained from melt and a parallel to such a freezing process does not take place during electrodeposition.

An ideal solid solution is the one in which the interatomic forces between unlike atoms are the same as those between like atoms. In such cases, no heat is evolved in mixing. The standard enthalpy is 0 and the Gibb's free energy change on the formation of such a solid solution (the standard chemical potential) of the alloy is determined by the entropy of mixing. For divalent metals, it is 9 mV and hence is neglected.²⁰



5 XRD pattern of Zn-Ni alloy, electrodeposited at 1 A dm⁻² and 55°C for 30 min

In the formation of intermetallic compounds, one would expect that small changes in composition can cause a rapid rise in free energy change. The free energy of formation of intermetallic phases can be calculated. Δ*E*, the difference in the anodic peak potential for both zinc and zinc alloys as a first approximation, was used to calculate the free energy of alloy formation. In the presence of sulphates, citrates and sulphamates, zinc forms complexes and the reversible potential of Zn/Zn (II) complex in the solution of its complex *E_r^{Zn}* is

$$E_r^{Zn} = E_{r,0}^{Zn} + \frac{2 \cdot 303RT}{2F} \log(a_{Zn \text{ complex}})$$

where *E_{r,0}^{Zn}* is the standard potential of the Zn/Zn (II) reaction.

The reversible potential of zinc in the alloy *E_{r,alloy}^{Zn}* is

$$E_{r,alloy}^{Zn} = E_{r,0}^{Zn} + \frac{2 \cdot 303RT}{2F} \log\left(\frac{a_{Zn \text{ complex}}}{a_{Zn, alloy}}\right)$$

$$\Delta E = -\frac{2 \cdot 303RT}{2F} \log(a_{Zn, alloy})$$

$$\Delta G = -2F\Delta E = -\frac{2 \cdot 303RT}{n} \log(a_{Zn, alloy})$$

Zinc-cobalt alloy

Table 2 presents the parameters derived from cyclic voltammograms at 20 mV s⁻¹. The existence of three

Table 2 Parameters derived from cyclic voltammograms for zinc dissolution from Zn-Co alloy film at *v*=20 mV s⁻¹*

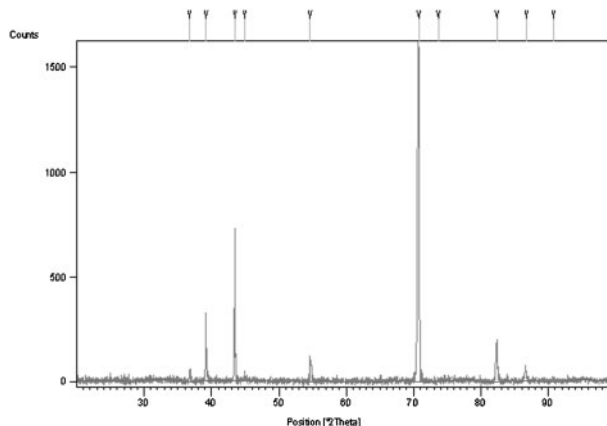
Zn/Co molar ratio in solution	<i>E_{p,a}</i> , mV (v. SCE)	Anodic peak intersection potential, mV (v. SCE)	-Δ <i>G</i> , kJ mol ⁻¹
1:0	-257	-1100	-
1:1	-650	-820	22.57
	-400	-700	30.09
	-140	-540	45.14

*Solution composition: 0.5M ZnSO₄, 0.5M CoSO₄ and 0.5M Na₂SO₄; SCE=saturated calomel electrode.

Table 4 Parameters derived from cyclic voltammograms for zinc dissolution from Zn-Ni alloy film at *v*=20 mV s⁻¹*

Zn/Co molar ratio in solution	<i>E_{p,a}</i> , mV (v. SCE)	Anodic peak intersection potential, mV (v. SCE)	-Δ <i>G</i> , kJ mol ⁻¹
0.9:1.0	-120	-900	-161.348
	+120	-	-
0.75:0.25	-80	-	-
	-10	-940	-129.16
0.5:0.5	-90	-1050	-40.337
0.25:0.75	-240	-1060	-32.269
1:0	-257	-1100	-

*Solution composition: zinc sulphamate (0.01<*x*<0.1M), nickel sulphamate (0.1<*x*<0.75M) and boric acid; SCE=saturated calomel electrode.



6 XRD pattern of Zn-Co alloy, electrodeposited at 1 A dm⁻² and 50°C for 30 min

planes of an intermetallic phase in Zn-Co alloy is suggested. From the total charges used for the alloy film formation, the dissolution peaks suggest that only a fraction of the alloy film has undergone dissolution (Table 3).

Zinc-nickel alloy

Increase in nickel ion concentration decreased the free energy of formation and a gradual change in Δ*G* with nickel ion concentration in solution suggests the presence of intermediate phases (Table 4). Dissolution rate of phases formed was found to be the maximum when the nickel ion concentration in solution was 0.25M (Table 5).

Zinc-iron alloy

Increase in iron ion concentration decreased the free energy of formation and a gradual change in Δ*G* with

Table 3 Charge flowed for dissolution of zinc from zinc-cobalt alloy film*

Zn/Co molar ratio in solution	<i>Q</i> , μC cm ⁻²
	385
	161
1:1	129.5

*Total charge flowed for the film formation=8800 μC cm⁻²; *Q*=dissolution rate per unit area.

Published by Maney Publishing (c) Institute of Metal Finishing

Table 5 Charge flowed for dissolution of zinc from zinc–nickel alloy film*

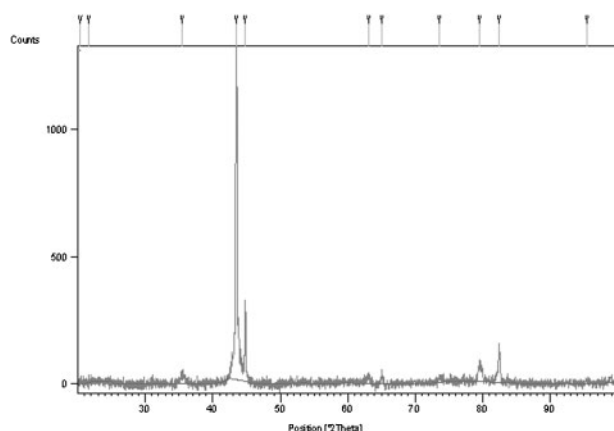
Zn/Ni molar ratio in solution	The first peak Q, $\mu\text{C cm}^{-2}$	The second peak Q, $\mu\text{C cm}^{-2}$
0.9 : 1.0	551.2	421.9
0.75 : 0.25	2127	3058
0.5 : 0.5	1960	2788
0.25 : 0.75	514.5	1200

*Total charge flowed for the film formation = 11 340 $\mu\text{C cm}^{-2}$; Q = dissolution rate per unit area.

Table 6 Parameters derived from cyclic voltammograms for zinc dissolution from Zn–Fe alloy film at $v=20\text{ mV s}^{-1}$ *

Zn/Fe molar ratio in solution	$E_{p,a}$, mV (v. SCE)	Anodic peak intersection potential, mV (v. SCE)	$-\Delta G$, kJ mole^{-1}
1 : 0	–257	–1100	–
1 : 0.01	–1020	–1046	–10.575
1 : 0.5	–850	–946	–30.137
1 : 1	–827	–936	–31.77
1 : 2	–800	–930	–33.27

*Solution composition: ferrous ammonium sulphate ($0.01 < x < 0.2\text{M}$), zinc sulphate ($0.01 < x < 0.2\text{M}$), 0.1M sodium sulphate and 0.05M triethanolamine; SCE = saturated calomel electrode.


7 XRD pattern of Zn–Fe alloy, electrodeposited at 1 A dm^{-2} and room temperature for 30 min
Table 7 Charge flowed for dissolution of zinc from zinc–iron alloy film*

Zn/Fe molar ratio in solution	Q, $\mu\text{C cm}^{-2}$
1 : 0.1	0.490
1 : 0.5	0.693
1 : 1	0.721
1 : 2	0.840

*Total charge flowed for the film formation = 8800 $\mu\text{C cm}^{-2}$; Q = dissolution rate per unit area.

Table 8 Parameters obtained from XRD data

Deposit	d spacing, angstrom		(hkl) plane	Inference
	standard	observed		
Zinc–nickel	2.09	2.10	(330)	$\delta\text{Ni}_3\text{Zn}_{22}$ (tetragonal)
	2.00	2.020	(214)	$\delta\text{Ni}_3\text{Zn}_{22}$ (tetragonal)
	1.452	1.471	(611)	$\text{Ni}_5\text{Zn}_{21}$ (cubic/bcc*)
	1.1689	1.134	(651)	$\text{Ni}_5\text{Zn}_{21}$ (cubic/bcc)
Zinc–cobalt	2.461	2.452	(102)	CoZn_{13} (monoclinic)
	2.098	2.085	(012)	
	2.077	2.055	(112)	
	1.329	1.326	(1002)	
Zinc–iron	2.301	2.452	(312)	FeZn_{13} (monoclinic)
	2.085	2.08	(122)	
	2.332	1.334	(800)	
	1.1717	1.1737	(1021)	
	1.1717	1.1737	(751)	

*bcc = body centred cubic.

iron ion concentration suggests the existence of inter-metallic phases (Table 6). Increase in iron content in the solution favoured the dissolution of zinc (Table 7).

XRD data analysis

The structures of electrodeposits formed according to conditions described in Table 1 were assessed by XRD studies (Figs. 5–7). The observed values are in good agreement with the standard values for the electrodeposited zinc transition metal alloys. The zinc–nickel alloy was found to contain $\delta\text{Ni}_3\text{Zn}_{22}$ (tetragonal) and $\text{Ni}_5\text{Zn}_{21}$ (cubic phases). CoZn_{13} (monoclinic phase) was seen in the zinc–cobalt alloy and FeZn_{13} (monoclinic) in zinc–iron deposits (Table 8).

Conclusions

Voltammetric studies were carried out on the deposition and dissolution of zinc–nickel, zinc–cobalt and zinc–iron alloy films. The deposition of zinc was found to involve stepwise reduction. The formation of monovalent zinc was found to be slow. The zinc alloy systems were found to be anomalous, resulting in a higher content of zinc in the film. Dissolution of zinc from the alloy film was observed. The dissolution was found to occur from intermediate phases, rich in zinc. From XRD data, $\delta\text{Ni}_3\text{Zn}_{22}$ and $\text{Ni}_5\text{Zn}_{21}$ in the zinc–nickel alloy deposit,

CoZn₁₃ in zinc–cobalt alloy deposit and FeZn₁₃ phases in the zinc–iron alloy deposit, were identified.

References

1. U. R. Evans: *J. Inst. Met.*, 1928, **40**, 99.
2. A. Glazunov: 'Metallic protective coatings', 1262; 1953, cited by A. R. Despic and V. D. Jovic in: 'Modern aspects of electrochemistry' (ed. R. E. White *et al.*), Vol. 27; 1995, NY, Plenum Press.
3. S. Swathirajan: *J. Electrochem. Soc.*, 1986, **133**, 671.
4. V. D. Jovic, R. M. Zejnilovic, A. R. Despic and J. S. Stevanovic: *J. Appl. Electrochem.*, 1988, **18**, 511.
5. V. D. Jovic, A. R. Despic, J. S. Stevanovic and S. Spaic: *Electrochim. Acta*, 1989, **43**, 1093.
6. V. D. Jovic, S. Spaic and A. R. Despic: *J. Electroanal. Chem.*, 1991, **310**, 391.
7. V. D. Jovic, S. Spaic, A. R. Despic, J. S. Stevanovic and M. Pristavec: *Mater. Sci. Technol.*, 1991, **7**, 1021.
8. V. S. Vasantha, M. Pushpavanam and V. S. Muralidharan: *Proc. Ind. Acad. Sci. Chem. Sci.*, 1995, **107**, 581.
9. C. L. Aravinda, V. S. Muralidharan and S. M. Mayanna: *J. Appl. Electrochem.*, 2000, **30**, 601.
10. D. R. Gabe: *Trans. IMF*, 1999, **77**, 213.
11. O. Giriene, R. Ramanauskas, P. Castro and P. Bartolo-Perez: *Trans. IMF*, 2001, **79**, (6), 1999.
12. M. Pushpavanam and M. Siluvai: *Trans. IMF*, 2004, **82**, (5–6), 174.
13. E. Ivaškevič, A. Selskis, A. Kaliničenko and R. Ramanauskas: *Trans. IMF*, 2004, **82**, (3–4), 93.
14. M. E. Bahrololoom, D. R. Gabe and G. D. Wilcox: *Trans. IMF*, 2004, **82**, (1–2), 51.
15. H. W. Pickering and C. Wagner: *J. Electrochem. Soc.*, 1967, **114**, 698.
16. R. S. Nicholson and I. Shain: *Anal. Chem.*, 1964, **36**, 706.
17. D. D. Macdonald: 'Transient techniques in electrochemistry', 193; 1977, New York, Plenum Press.
18. A. Brenner: 'Electrodeposition of alloys, principles and practice', Vol. 2; 1963, New York, Academic Press.
19. M. J. Nicol and H. I. Philip: *J. Electroanal. Chem.*, 1976, **70**, 803.
20. D. A. Porter and Y. A. Easterling: 'Phase transformations in metals and alloys'; 1980, Wokingham, Van Nostrand Reinhold.